Formation of self-sealing capability for carbon dioxide sequestration site in shallow sub-seabed sediments by three-phase coexistence

Jiangzhi Chen and Shenghua Mei

CAS Key Laboratory for Experimental Study under Deep-sea Extreme Conditions
Institute of Deep Sea Science and Engineering, Chinese Academy of Sciences
Sanya, Hainan Province 572000

Key Points:

- Enhanced CO2 migration from sequestration site by liquid CO2 seeping through marine sediments facilitates fast CO2 hydrate formation.
- Coexisting CO2 bubbles and hydrates in the three-phase zone reduces sediment layer permeability even at low hydrate saturation level.
- Temperature and pressure perturbations may affect the three-phase zone, making the sealing capability prone to earthquakes or landslides.

Corresponding author: Jiangzhi Chen, chenjz@idsse.ac.cn

Abstract

Storing CO_2 in sub-seabed sediment is a promising CO_2 sequestration method to reduce the atmospheric CO_2 concentration and mitigate climate change, with the advantage of self-sealing capability due to formation of CO_2 hydrate in the sediment pore space. Above the sequestration site, enhanced CO_2 migration and supersaturation lead to a zone of coexisting gaseous, hydrate and aqueous phases of CO_2 where curved surfaces of bubbles and hydrate crystals shift the phase equilibria, enabling fast development of the self-sealing capability due to permeability reduction by both hydrates and entrapped bubbles. We simulate the three-phase zone in a shallow seabed using a Monte Carlo method in packed synthetic mono-dispersed spherical sediment grains, and analyze its variations due to temperature and pressure perturbations. Our work demonstrates the difference between CO_2 hydrate-bearing sediment layer and methane hydrate reservoir, and provides insight into the formation mechanisms of the self-sealing cap above sequestration sites.

Plain Language Summary

Removing carbon dioxide from the atmosphere and storing it in geological formations is a promising method to mitigate global climate change. People have proposed that injecting liquid carbon dioxide into sub-seabed formations can take the advantage of carbon dioxide hydrate forming in the low-temperature high-pressure environment, which can serve as a sealing cap to prevent carbon dioxide leakage. However, treating the formation of carbon dioxide hydrate cap similar to the formation of methane hydrate reservoir neglects the thermodynamic difference between carbon dioxide and methane, and overlooks the role of carbon dioxide bubbles in the marine sediments. Abundant liquid carbon dioxide seepage from the storage site drives fast carbon dioxide migration to a depth near the hydrate stability zone, and unlike methane, carbon dioxide becomes supersaturated as it migrates upwards. The supersaturated carbon dioxide has to become gas bubbles and hydrates. Sediment pores enable the carbon dioxide bubbles, hydrates and dissolved carbon dioxide to form a three-phase zone, where entrapped gas bubbles and hydrate crystals occupy the pore space, and reduce the sediment permeability. The sealing capability of the cap not only depends on the hydrate-bearing sediment layer, but also on the gas bubbles filling the pore spaces.

1 Introduction

The concentration of CO_2 in the atmosphere has been steadily increasing since the industrial revolution because of human activity. According to the IPCC report Climate Change 2021 (Masson-Delmotte et al., 2021), the global CO_2 concentration in 2019 was 410 ppm, the highest in the last two million years, accompanied by an increased frequency of extreme weather events worldwide. Only with drastically reduced emissions can the global temperature rise be limited to less than 2 °C, and to less than 1.5 °C by the end of the century if zero-emissions are achieved by 2050. This environmental pursuit has driven the investigation of carbon capture, sequestration and storage (CSS), which removes and stores CO_2 from the atmosphere.

It is suggested that regardless of the storage method, after 100 years, the retained fraction of CO_2 is approximately between 65 – 100 %, and after 500 years the fraction drops to 30 – 85 % (Metz et al., 2005), so CSS methods with efficient leakage prevention are especially favored. Among all CSS methods, storing CO_2 in sub-seabed sediments (Koide et al., 1997) has drawn much attention because of its advantage of self-sealing. Liquid CO_2 is injected into sub-seabed formations (Shukla et al., 2010), and under low-temperature high-pressure conditions, the injected CO_2 can form CO_2 hydrates. Gas hydrates are ice-like compounds in which water molecules connected by hydrogen bonds form cages, and smaller gas molecules (guests), such as CO_2 and methane, are trapped inside the cages, which are commonly found in permafrost regions and marine sediments (Sloan & Koh, 2007). In sediments, CO_2 hydrates exist in the sediment pores near the base of the CO_2 hydrate stability zone (BHSZ). The CO_2 hydrate can reduce the porosity of the sediments, block the flow of the pore fluid, and decrease the permeability (e.g., Tohidi et al., 2001). Therefore, the hydrate-bearing sediment layer is self-sealing, which ensures long-term stability (Eccles & Pratson, 2012) and has great potential to mitigate global warming (Adams & Caldeira, 2008; Goldberg et al., 2008).

Compared with other CSS technologies, such as storing CO_2 in geological formations on land, further knowledge of the formation of the self-sealing hydrate-bearing sediment layer is needed before the CO_2 sequestration using the hydrate can be deployed. Specifically, the formation process that the hydrate layer and its sensibility to possible temperature and pressure perturbations are required for better understanding the sealing efficiency and stability. Previous works mainly focused on the formation of methane hydrate reservoir (e.g., Rempel & Buffett, 1997; Burwicz et al., 2017; Nole et al., 2018; You & Flemings, 2021) and its responses to natural temperature fluctuations (e.g., Reagan & Moridis, 2008; Sultan et al., 2004) or during exploitation (e.g., Rutqvist & Moridis, 2009; Waite et al., 2009), but given the thermodynamic difference between methane hydrate and CO_2 hydrate, the results for methane hydrate cannot be readily applied to the CO_2 hydrate. For example, the models of methane hydrate reservoir formation (e.g., Rempel & Buffett, 1997; You & Flemings, 2021) indicate that it requires tens of thousands of years for the methane hydrate to reach moderate saturation (fraction of sediment pore space occupied by the hydrate), evidently unsuitable for the formation of self-sealing cap above the CO_2 sequestration site where a large amount of CO_2 keeps upwelling. Also, the CO_2 hydrate has a much narrower stability range compared with that of the methane hydrate (Sloan & Koh, 2007), thus the CO_2 hydrate reservoir is more sensitive to temperature and pressure perturbations. Therefore, we need to study how the self-sealing capability develops in the sediments, and how the differences affect the leakage prevention and stability of the cap.

In this study, we investigated the formation of a self-sealing CO_2 hydrate cap near the BHSZ above the sequestration site. For simplicity, the sequestration reservoir is treated as a CO_2 source at a representative depth at 800 mbsf, which is the depth for the Sleipner site in Norway and Enping site in China. The sediment layers above the site do not deform during the phase change of liquid CO_2, i.e., no fracturing caused by invasion of the gaseous phase or impingement of the hydrate phase. We first revisit the existing model on advection-diffusion driven methane hydrate reservoir formation, and then model the CO_2 hydrate cap formation considering the seeping transport of CO_2 from the source of liquid CO_2, and the coexistence of the CO_2 bubble, CO_2 hydrate and dissolved CO_2 in aqueous solutions, where phase equilibria are shifted due to heterogeneously distributed surface curvatures. The sensitivity of the three-phase coexisting zone to the temperature and pressure perturbations is quantitatively evaluated. Before concluding, we discuss how the three-phase zone serves as an effective sealing cap with fast-developing sealing capability, as well as the role of the CO_2 bubbles in the sediment pore space. The parameters used in this study are listed in Table 1.

2 Formation of self-sealing cap

Under bulk conditions, the depth of the BHSZ is determined by the three-phase equilibrium of free CO_2 gas (G), CO_2 hydrate (H), and dissolved CO_2 in aqueous solutions (L), constrained by pressure, temperature, and salinity (e.g., Sloan & Koh, 2007). In pure water, CO_2 hydrates have a pressure range of $1-4.5$ MPa and a temperature range of $272-283$ K (Sun & Duan, 2005), and in seawater the salinity may cause a temperature depression of about 1.5 K (Dickens & Quinby-Hunt, 1994). Above the maximum pressure, CO_2 is a supercritical liquid (L_{CO_2}) and cannot form stable hydrates. Based on the stability conditions of CO_2 hydrate, there are two different CSS strategies using CO_2 hydrate: in a shallow seabed with a water depth of less than 300 m, CO_2 may exist as hydrates; in a deep seabed supercritical liquid CO_2 may be sealed by a CO_2 hydrate cap above (Koide et al., 1997). The first strategy is favored due to technical and economic considerations, and depleted oil or gas reservoirs can be used as storage sites. In both cases, because the surface tension between liquid CO_2 and water is significantly less than that between oil and water, CO_2 leakage is inevitable (Li et al., 2006; Espinoza & Santamarina, 2010).

2.1 Hydrate formation by fluid advection

In the widely used model (e.g., Rempel & Buffett, 1997; Daigle & Dugan, 2011; You et al., 2019), CO_2 molecules from the source at z_s are transported to the BHSZ at a depth of z_3 by upward flow advection and diffusion. The Péclet number is $\mathrm{Pe} = (z_s - z_3)u_l/D_g$ where $z_s - z_3$ is the characteristic length from the CO_2 source to the BHSZ, typically about 500 m for shallow seabed carbon dioxide sequestration site at 800 mbsf, the pore fluid upwelling velocity u_l is usually less than 1 mm/yr (Davie & Buffett, 2003), and the effective diffusion coefficient D_g through the sediments is about $10^{-9}\,\mathrm{m^2/s}$. The Péclet number $\mathrm{Pe} \gg 1$, so that the advection dominates the CO_2 transport, and the diffusion term can be ignored. The hydrate is slowly accumulating so the variation of CO_2 concentration X (in mass fraction) in pore fluid $\partial X/\partial t$ can be ignored. The simplified mass conservation in 1D with a downward z direction is

$$\frac{\partial S_h}{\partial t} = \frac{u_l}{\xi_h \phi (f - X + fX)} \left.\frac{\partial X}{\partial z}\right|_{z_3} \tag{1}$$

where $\xi = \rho_h/\rho_l$ is the ratio of the CO_2 hydrate density to seawater density, ϕ is the porosity, and $f = 0.289$ is the mass fraction of CO_2 in sI CO_2 hydrate with $n \approx 6$. The equation is the same as in Rempel and Buffett (1997) if the higher order term fX is ignored, and the timescale is

$$\frac{\xi_h \phi (f - X)}{u_l} \left(\left.\frac{\partial X}{\partial z}\right|_{z_3} \right)^{-1}. \tag{2}$$

At the BHSZ, the CO_2 concentration X is determined by the H-L equilibrium, and can be converted from the molar fraction x_{hl} such that

$$\frac{\partial X}{\partial z} = \frac{X(1-X)}{1 - x_{hl}} \frac{\partial \ln x_{hl}}{\partial z}, \tag{3}$$

To evaluate $\partial \ln x_{hl}/\partial z$ for the H-L equilibrium,

$$\mathrm{CO_2(aq)} + n\,\mathrm{H_2O} \rightleftharpoons \mathrm{CO_2} \cdot n\,\mathrm{H_2O\,(s)}, \tag{4}$$

we use the thermodynamic relations

$$\left.\frac{\partial \ln x_{hl}}{\partial T}\right|_P = \frac{\Delta^{hl}_{\mathrm{sol}} H}{RT^2} > 0, \quad \left.\frac{\partial \ln x_{hl}}{\partial P}\right|_T = \frac{V_h - \bar{V}_g - nV_w}{RT} < 0, \tag{5}$$

where R is the ideal gas constant, $\Delta^{hl}_{\mathrm{sol}} H$ is the hydrate dissolution heat, V_h is the molar volume of CO_2 hydrate, $\bar{V}_g$ is the partial molar volume of dissolved CO_2, and V_w is the molar volume of water. The bulk BHSZ is at depth z_3 below the seafloor, corresponding to a three-phase equilibrium condition

$$T_3 = T_0 + G_T z_3, \quad P_3 = P_0 + G_P z_3, \tag{6}$$

where T_0 and P_0 are the temperature and pressure at the seafloor, and G_T and G_P are the geothermal gradient and hydrostatic pressure gradient in the sediment, respectively. The CO_2 solubility vary with the depth near z_3 according to

$$g_{hl} = \left.\frac{\mathrm{d} \ln x_{hl}}{\mathrm{d}z}\right|_{z_3} = \frac{\Delta^{hl}_{\mathrm{sol}} H}{RT_3^2} G_T + \frac{V_h - \bar{V}_g - nV_w}{RT_3} G_P. \tag{7}$$

With the three-phase equilibrium $T_3 \approx 282\,\mathrm{K}$ and $P_3 \approx 4\,\mathrm{MPa}$, and use nominal values for G_T and G_P (Table 1) we have

$$g_{hl} = 1.909\,\mathrm{km}^{-1}. \tag{8}$$

From eq. (2), with $X \approx 0.0609$ (Duan & Sun, 2003), $u_l \approx 1\,\mathrm{mm/yr}$, and the value of g_{hl}, we can find that it takes about 10^4 yr for S_h from zero to increase to 1%, which is reasonable for natural hydrate deposits, but too slow for the formation of self-sealing hydrate cap. Other proposed hydrate growth mechanisms, such as the burial-driven recycling (Burwicz et al., 2017; Nole et al., 2018; You & Flemings, 2021; Schmidt et al., 2022) may help to build high saturation of hydrate at later stage after enough CO_2 is transported to the BHSZ.

It is evident that if CO_2 transport is through pore fluid advection similar to methane, building up a hydrate reservoir by advection-dominated hydrate accumulation occurs at a geological timescale. However, for CO_2 sequestration site, given the fact that abundant CO_2 exists merely hundreds of meters below the hydrate stability zone, formation of the sealing cap can benefit from enhanced CO_2 migration, shifted phase equilibria in porous sediment, and reduced permeability caused by entrapped CO_2 bubbles and hydrate crystals in the sediment, and require significantly less time.

2.2 Enhanced CO_2 migration by liquid CO_2 seepage

With a shallow water depth $d = 100\,\mathrm{m}$, a geothermal gradient $G_T = 0.03\,\mathrm{K/m}$ and a hydrostatic pressure gradient $G_P \approx 10^4\,\mathrm{Pa/m}$, the base of the hydrate stability zone is at $z_3 = 288\,\mathrm{mbsf}$, and the CO_2 liquid–gas phase boundary is at $z_v = 352\,\mathrm{mbsf}$ (Figure 1a). Liquid CO_2 from the sequestration site first permeates to z_v by ambient pressure and buoyancy, which can be approximated as a Darcy flow

$$\mathbf{u}_{\mathrm{CO_2}} = -\frac{k}{\mu_{\mathrm{CO_2}}}\boldsymbol{\nabla}(P - \rho_{\mathrm{CO_2}}\mathbf{g}) \tag{9}$$

and compared with the pore fluid upwelling velocity without CO_2

$$\mathbf{u}_l = -\frac{k}{\mu_l}\left(\boldsymbol{\nabla}P - \rho_l\mathbf{g}\right) \tag{10}$$

we have

$$\mathbf{u}_{\mathrm{CO_2}} = \frac{\mu_l}{\mu_{\mathrm{CO_2}}}\mathbf{u}_l + \frac{k}{\mu_{\mathrm{CO_2}}}(\rho_{\mathrm{CO_2}} - \rho_l)\mathbf{g}. \tag{11}$$

The density difference $\Delta\rho = \rho_{\mathrm{CO_2}} - \rho_l$ between liquid CO_2 and the seawater can be calculated using the correlation by Levine et al. (2007) (Figure 1b), the permeability of the sediment to liquid CO_2 k is assumed the same as the permeability to water, and the viscosity of the liquid CO_2 is from Fenghour et al. (1998). The pore fluid upwelling velocity is taken as $1\,\mathrm{mm/yr}$ (Davie & Buffett, 2003). At the temperature and pressure range of the model, the liquid CO_2 upwelling velocity is around $0.7\,\mathrm{m/yr}$, about two orders of magnitude larger than u_l, and for a unit seep area, the advection mass flux of CO_2 is less than $u_l\rho_l X \approx 0.06\,\mathrm{kg/(m^2{\cdot}yr)}$, whereas the liquid CO_2 seepage can transport $u_{\mathrm{CO_2}}\rho_{\mathrm{CO_2}} \approx 608\,\mathrm{kg/(m^2{\cdot}yr)}$. In fact, if we take into account of possible overpressure during the injection of liquid CO_2, the permeation can be even faster.

With the enhanced permeation of liquid CO_2, at the $\mathrm{L_{CO_2}}$-G boundary which is only at a distance $z_v - z_3 = 64.5\,\mathrm{m}$ from the bulk BHSZ, abundant liquid CO_2 turns into gaseous (and dissolved) CO_2. This distance is only a tenth of the distance from the BHSZ to the sequestration depth, drastically shorter compared with that of methane migration from deep methanogenic regions to the BHSZ for methane, but it still requires a long time if CO_2 can only form hydrate at the BHSZ. However, due to shifted G-L and H-L equilibria in sediment pores, a three-phase zone where CO_2 bubbles, CO_2 hydrate

Table 1. Parameters and nominal values for CO_2 gas, CO_2 hydrate, and water based on homogeneous three-phase equilibrium conditions $T_3 = 282\,\mathrm{K}$ and $P_3 = 4\,\mathrm{MPa}$.

	Model parameters	Symbol	Unit	Value
thermodynamic parameters	CO_2 molar dissolution heat [a]	$\Delta_{\mathrm{sol}}^{gl}H$	kJ/mol	-20.24
	CO_2 hydrate molar dissolution heat [b]	$\Delta_{\mathrm{sol}}^{hl}H$	kJ/mol	42.3
	molar volume of water [c]	V_w	$\mathrm{cm^3/mol}$	17.93
	partial molar volume of CO_2 in water [a]	$\bar{V}_g$	$\mathrm{cm^3/mol}$	28.4
	molar volume of CO_2 hydrate [d]	V_h	$\mathrm{cm^3/mol}$	135.4
	G-L surface tension	γ_{gl}	$\mathrm{J/m^2}$	0.07
	H-L surface tension [e]	γ_{hl}	$\mathrm{J/m^2}$	0.029
	hydration number	n	–	~ 6
	mass fraction of CO_2 in hydrate	f	–	0.289
	molar fraction of CO_2 in G-L equilibrium	x_{gl}	–	
	molar fraction of CO_2 in H-L equilibrium	x_{hl}	–	
	mass fraction of CO_2 in H-L equilibrium	X	–	
	compressibility factor of CO_2 [f]	Z	–	
hydraulic parameters	geothermal gradient	G_T	K/m	3×10^{-2}
	hydrostatic pressure gradient	G_P	Pa/m	10^4
	seawater density [g]	ρ_l	$\mathrm{kg/m^3}$	1029
	liquid CO_2 density	ρ_{CO_2}	$\mathrm{kg/m^3}$	
	CO_2 hydrate density [h]	ρ_h	$\mathrm{kg/m^3}$	1120
	water viscosity	μ_l	$\mathrm{Pa \cdot s}$	0.001
	liquid CO_2 viscosity [i]	μ_{CO_2}	$\mathrm{Pa \cdot s}$	
	pore fluid upwelling velocity	u_l	mm/yr	1
	liquid CO_2 upwelling velocity	u_{CO_2}	mm/yr	
	sediment permeability	k	$\mathrm{m^2}$	10^{-15}
	effective gas diffusion coefficient	D_g	$\mathrm{m^2/s}$	10^{-9}
	effective salt diffusion coefficient	D_s	$\mathrm{m^2/s}$	10^{-9}
	volume fraction of hydrate in pores	S_h	–	
	volume fraction of gas in pores	S_g	–	
	volume fraction of liquid in pores	S_l	–	
geological parameters	sequestration site depth	z_s	mbsf	800
	water depth	d	m	100
	bulk BHSZ depth [j]	z_3	mbsf	288
	L_{CO_2}-G boundary [k]	z_v	mbsf	352
	sediment porosity	ϕ	–	0.5
	seafloor temperature	T_0	°C	0.5

Sources:
[a] Duan and Sun (2003). The dissolution heat is evaluated at T_3, where the negative sign means that the solution releases heat, close to the value by Carroll et al. (1991). The partial molar volume of CO_2 is calculated as the derivative of the chemical potential of CO_2 with respect to the temperature. [b] The sum of the molar dissociation heat of CO_2 hydrate into water and CO_2 gas $\Delta_{\mathrm{dis}}H = 63.6\,\mathrm{kJ/mol}$ (Anderson, 2003) and CO_2 dissolution heat $\Delta_{\mathrm{sol}}^{gl}H$. [c] Wagner and Pruss (1993) [d] Sun and Duan (2005) [e] Hardy (1977) [f] Peng and Robinson (1976) [g] Spivey et al. (2004) [h] Udachin et al. (2001) [i] Fenghour et al. (1998) [j] Calculated using Wendland et al. (1999). [k] Calculated using Nevers (2012).

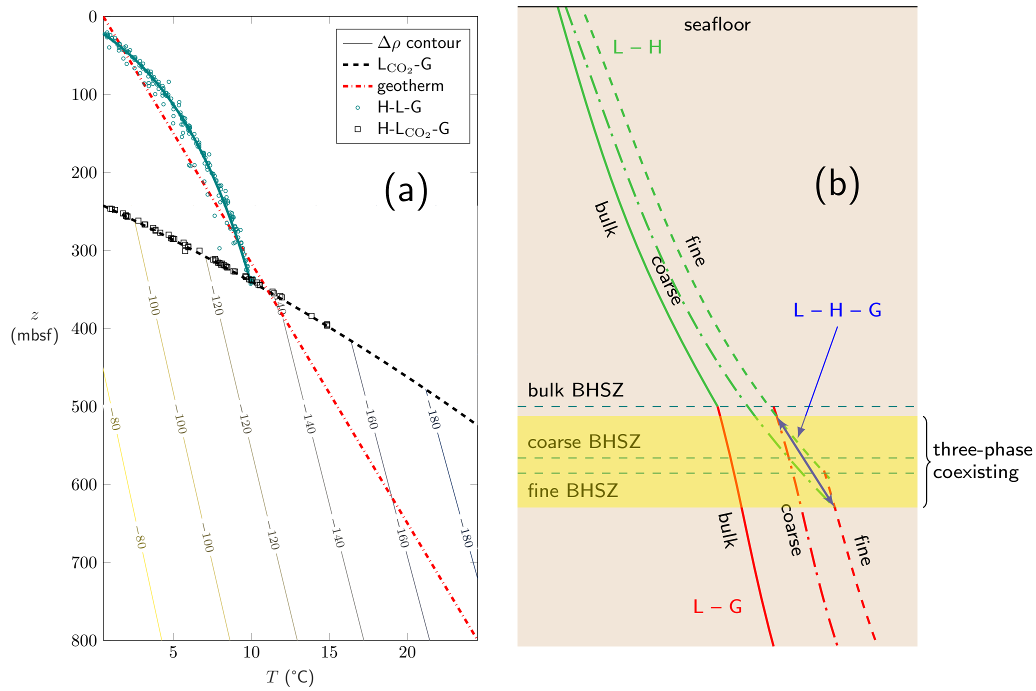

Figure 1. (a) The hydrate stability zone in the sediment, defined by the three-phase equilibrium of CO_2 hydrate, gaseous CO_2 and aqueous CO_2 (teal circles and curve, with data compiled by Sloan and Koh (2007)) and the geothermal temperature (red dashed line). The black dashed line is the boundary between liquid CO_2 and gaseous CO_2, which is also the three-phase equilibrium of CO_2 hydrate, gaseous CO_2 and liquid CO_2 (black squares, from Larson (1955)). The contour of the density difference between liquid CO_2 and seawater $\Delta\rho = \rho_{CO_2} - \rho_l$ with a constant salinity 3.5 % (Levine et al., 2007) overlayed on the temperature profile below the L_{CO_2}-G boundary. The contour levels are in kg/m^3. In the temperature and pessure range considered, $\Delta\rho$ is around $-160\,kg/m^3$. (b) The three-phase coexisting zone near the BHSZ. Under bulk conditions, above the BHSZ, the CO_2 solubility is determined by H-L equilibrium, increasing with the depth (green curves). Below the BHSZ, hydrate dissociates and the dissolved CO_2 is in equilibrium with CO_2 gas (red curves). The shifted solubilities in pores help to generate a finite zone where three phase coexist, where one non-wetting phase in finer pores with larger surface curvatures is in equilibrium with the other non-wetting phase in coarser pores with smaller surface curvatures.

and aqueous CO_2 coexist may extend towards the L_{CO_2}-G boundary. As a result, the gaseous and dissolved CO_2 may turn into CO_2 hydrate crystals without further migration, and the entrapped CO_2 bubbles and hydrate crystals can significantly reduce the permeability even at relatively low hydrate saturations.

3 Three-phase coexistence near the BHSZ

The depth of the BHSZ in bulk conditions is determined by the intersection of H-L and G-L equilibria constrained by the temperature, pressure, and salinity conditions, and below the BHSZ the hydrate phase is no longer stable. In porous sediments, however, the formation of hydrate deviates from the L-G-H three-phase bulk equilibrium (Figure 1b). The aqueous solution wets the sediment grains, and gaseous and hydrate phases are both non-wetting to the grains. Pore walls act as geometric constraints to surfaces of gas bubbles and hydrate crystals, and hence affect the curvatures and the surface energy of the curved H-L or G-L interfaces (e.g., Clennell et al., 1999; Henry et al., 1999; Daigle & Dugan, 2011; Liu & Flemings, 2011).

Existing studies on the hydrate in porous media mostly treated the pores as cylinders (e.g., Wilder et al., 2001) or spheres connected by cylindrical throats (e.g., Liu & Flemings, 2011). These simplified regular pore models help to understand the effect of pore size distribution on the equilibrium of hydrate in porous media, but they ignore the variation of the interface curvature of the non-wetting phases, which shifts the equilibrium as non-wetting phases grow or dissolve. In real marine sediment, pore space between granular sediment grains is irregular, and allows phase boundaries of different curvatures to coexist in adjacent pores and crevices. To accommodate the pore sizes, the bulk BHSZ shifts to a finite three-phase zone due to heterogeneously distributed interface curvatures in the sediments, where one non-wetting phase in the pore center with a large interface radius may be in equilibrium with the other non-wetting phase in a small crevice with a small interface radius at the same pressure, temperature and salinity.

3.1 Thermodynamic relations

To investigate the shifted solubilities in pores, we use x_{gl} and x_{hl} to denote the equilibrium CO_2 solubilities (in molar fraction) at a three-phase equilibrium temperature T_3 and pressure P_3 with a flat G-L and H-L interface. The elevated CO_2 solubilities with a gas bubble radius r_g or a hydrate crystal radius r_h are

$$x'_{gl}(r_g) = x_{gl}\left(1 + \frac{\gamma_{gl}}{P_3 + G_P\Delta z}\frac{2}{r_g}\right), \quad x'_{hl}(r_h) = x_{hl}\exp\left[\frac{2V_h\gamma_{hl}}{Rr_h(T_3 + G_T\Delta z)}\right]. \tag{12}$$

where γ_{gl} and γ_{hl} are the surface tension of the G-L and H-L surfaces, and Δz is the offset from the bulk BHSZ depth z_3. Similar to the H-L equilibrium in Section 2.1, in the G-L equilibrium

$$\mathrm{CO_2(g)} \rightleftharpoons \mathrm{CO_2(aq)}, \tag{13}$$

the thermodynamic relations for the CO_2 solubility are

$$\left.\frac{\partial \ln x_{gl}}{\partial T}\right|_P = \frac{\Delta_{\mathrm{sol}}^{gl}H}{RT^2} < 0, \quad \left.\frac{\partial \ln x_{gl}}{\partial P}\right|_T = \frac{V_g - \bar{V}_g}{RT} \approx \frac{Z}{P} > 0, \tag{14}$$

where $\Delta_{\mathrm{sol}}^{gl}H$ is the molar heat of solution of CO_2 gas, V_g is the molar volume of CO_2 gas, $\bar{V}_g$ is the partial molar volume of CO_2 in water, which is negligible compared with V_g, and Z is the compressibility factor of CO_2. Partial pressure from water vapor is also negligible because in the temperature range of interest, the saturation vapor pressure is much smaller than the hydrostatic pressure. The dependence of G-L solubility x_{gl} with depth near z_3 can be expressed in a form similar to eq. (7)

$$g_{gl} = \left.\frac{\mathrm{d}\ln x_{gl}}{\mathrm{d}z}\right|_{z_3} = \frac{\Delta_{\mathrm{sol}}^{gl}H}{RT_3^2}G_T + \frac{Z}{P_3}G_P, \tag{15}$$

where Z is evaluated using an equation of state for CO_2 (e.g., Peng & Robinson, 1976). With $T_3 \approx 282\,\mathrm{K}$, $P_3 \approx 4\,\mathrm{MPa}$, and the values for G_T and G_P (Table 1) we have

$$g_{gl} = 0.778\,\mathrm{km}^{-1} \tag{16}$$

Because $g_{hl} = 1.913\,\mathrm{km}^{-1} > g_{gl}$, the gradient of the CO_2 G-L solubility is much gentler than that of the CO_2 H-L solubility, and the positive values mean that both increase with the depth. Within a small distance of z_3, the change in Z and other thermodynamic properties are negligible, and bulk solubilities at $z = z_3 + \Delta z$ are approximated as

$$x_{gl}(z) = x_3\exp\left(g_{gl}\Delta z\right), \quad x_{hl}(z) = x_3\exp\left(g_{hl}\Delta z\right), \tag{17}$$

and the resulting change in the BHSZ location from the bulk BHSZ is determined by equating the two solubilities at $z = z_3 + \Delta z$

$$\frac{2V_h\gamma_{hl}}{r_h R(T_3 + G_T\Delta z)} = (g_{gl} - g_{hl})\,\Delta z + \ln\left(1 + \frac{2\gamma_{gl}}{r_g}\frac{1}{P_3 + G_P\Delta z}\right). \tag{18}$$

With r_g and r_h constrained by the pore space, the depth offset Δz can be solved. We can use a Monte Carlo method to find the maximum offset for mono-dispersed granular sediment as a function of the saturation levels.

3.2 Monte Carlo simulation of the three-phase boundaries

To account for the distribution of curved interfaces in 3D irregular pores between spherical grains, we use the method in Chen et al. (2021) to study the L-G-H three-phase coexistence in marine sediments, which was based on the Monte Carlo approach by Rempel (2012) in 2D crevice spaces and later extended to 3D by Chen et al. (2020). A description of the Monte Carlo scheme is provided in the Supporting Information. For simplicity, we use the mono-dispersed Finney pack (Finney, 1970), and ignore possible influence of the salinity because with small variations in the salinity, the temperature depression is almost uniform near the BHSZ. We calculated the deviations from the bulk BHSZ corresponding to the radii of the gas bubbles and hydrate crystals using eq. (18), shown in Figure 2 with the positive direction pointing downwards. The spherical grain radii are $R = 10^{-6} - 10^{-4}$ m, in the grain size range of silt to fine sand. For both grain sizes, the three-phase zones bend downwards at high saturation levels of the emergent phase, because the growing emergent phase further intrudes into the crevice, increasing both curvatures. In coarser sediment (10^{-4} m grain radius) with larger pores, the three-phase zone is thinner and closer to the bulk BHSZ, whereas in finer sediments (10^{-5} m and 10^{-6} m grain radius), the three-phase zone is broader, suggesting stronger deviations from the bulk conditions. For finer grains, the three-phase zone extend significantly towards the L_{CO_2}-G boundary even at relatively low hydrate saturations. Therefore, CO_2 can form hydrate crystals near the L_{CO_2}-G boundary without migrating a long distance to the bulk BHSZ. These hydrate crystals, together with entrapped CO_2 bubbles, help to limit the leakage even before sufficient hydrates accumulate and form a hydrate sealing cap.

3.3 Sensitivity of the three-phase zone to temperature and pressure perturbations

With the three-phase zone acting as a bubble-hydrate buffer, it is important to understand the response of the zone to temperature and pressure perturbations. Because the variation in the hydrostatic pressure gradient G_P is negligible, the depth of the three-phase zone depends on the geothermal gradient G_T and the three-phase equilibrium conditions T_3 and P_3 which are functions of the water depth d and G_T. Therefore, the main source of perturbations for the three-phase zone is the change of the sea level and temperature perturbations. We perform numerical tests with the sediment grain radius 10^{-5} m, where the seawater depth $d = 90 - 110$ m and the geothermal gradient $G_T = 25 - 35$ K/km. The results are presented in Figure 3. Combined with Figure 2, we can see that finer grains, larger geothermal gradients, and shallower water depths all tend to broaden the three-phase zone. In the scenario of $d = 90$ m and $G_T = 3.5\times10^{-2}$ K/m, the three-phase zone is so broad that it encompasses the L_{CO_2}-G boundary, which means that CO_2 hydrates can coexist with CO_2 bubbles immediately after the liquid CO_2 turns into gaseous CO_2. Sources of the perturbations could be seasonal temperature changes or tidal sea level changes, but sub-marine geologic activities, such as earthquakes or landslides, are more likely to cause large abrupt changes in a short period of time, which can affect the sealing capability of the bubble-hydrate cap.

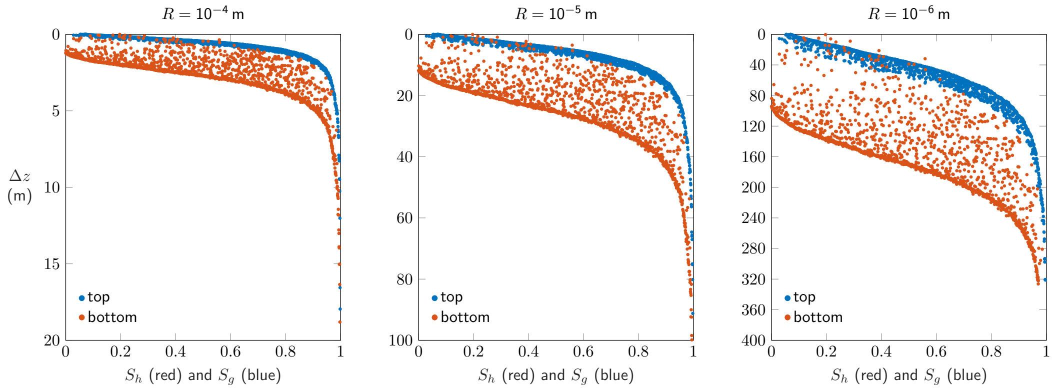

Figure 2. Monte Carlo simulation of the upper and lower boundaries of the three-phase zone for CO_2 hydrate bearing sediments plotted against the saturation of the emerging phase in 3D mono-dispersed granular media with particle sizes $R = 10^{-4} - 10^{-6}$ m. At the bottom boundary the emerging phase is the hydrate, whereas at the top boundary the gaseous phase is incipient. With larger sediment grains of a grain radius 10^{-4} m, the three-phase zone in sediments is closer to the bulk BHSZ, and its thickness is much less than that of 10^{-5} m and 10^{-6} m grain radius, consistent with the fact that if the phase equilibrium is not confined by the finite pores, the three-phase zone shrinks to a unique depth, i.e., the bulk BHSZ.

4 Discussion

4.1 Permeability reduction due to entrapped bubbles

In the sediment, the sealing capability is usually attributed to the hydrate saturation S_h. However, the role of entrapped CO_2 bubbles cannot be overlooked. To reduce the surface energy, small mobile bubbles tend to grow and coalesce into a large bubble during upwelling, and the large bubble is eventually confined by pore walls and occupies significant fraction of the pore space. Below the three-phase zone, the bubble-filled pore space may also reduce the liquid saturation S_l, hence reduce the permeability. Inside the three-phase zone, the saturations of hydrate crystals and gas bubbles are in a dynamic equilibrium, and both the pore centers and crevices are occupied by the non-wetting phases. Consequently, the permeability is further reduced.

4.2 Increasing CO_2 supersaturation during upwelling

The gas solubility plays an important role in determining the location of the three-phase zone and gas transport below the BHSZ. For CO_2, we have calculated that at the BHSZ $\partial \ln x_{gl}/\partial z = 0.778\,\mathrm{km}^{-1} > 0$, which means that the CO_2 gas solubility increases with the depth, because the contribution from increasing pressure outweighs the decreasing solubility from higher temperature. At the $\mathrm{L}_{\mathrm{CO_2}}$-G boundary about 100 m from the BHSZ, x_{gl} is about 8% higher than that near the BHSZ. The solubility difference not only provides a gradient for diffusion, but also causes increasing CO_2 supersaturation during the upwelling, and more bubbles form. Besides permeability changes, the bubble-filled column below the BHSZ may also affect the chemistry of the pore fluid. It is worth noting that for methane, the gas solubility decreases with the depth below the BHSZ (Chen et al., 2021), so the supersaturation level of methane decreases as it migrates towards the BHSZ, which is another important difference between methane hydrate reservoir and CO_2 hydrate reservoir.

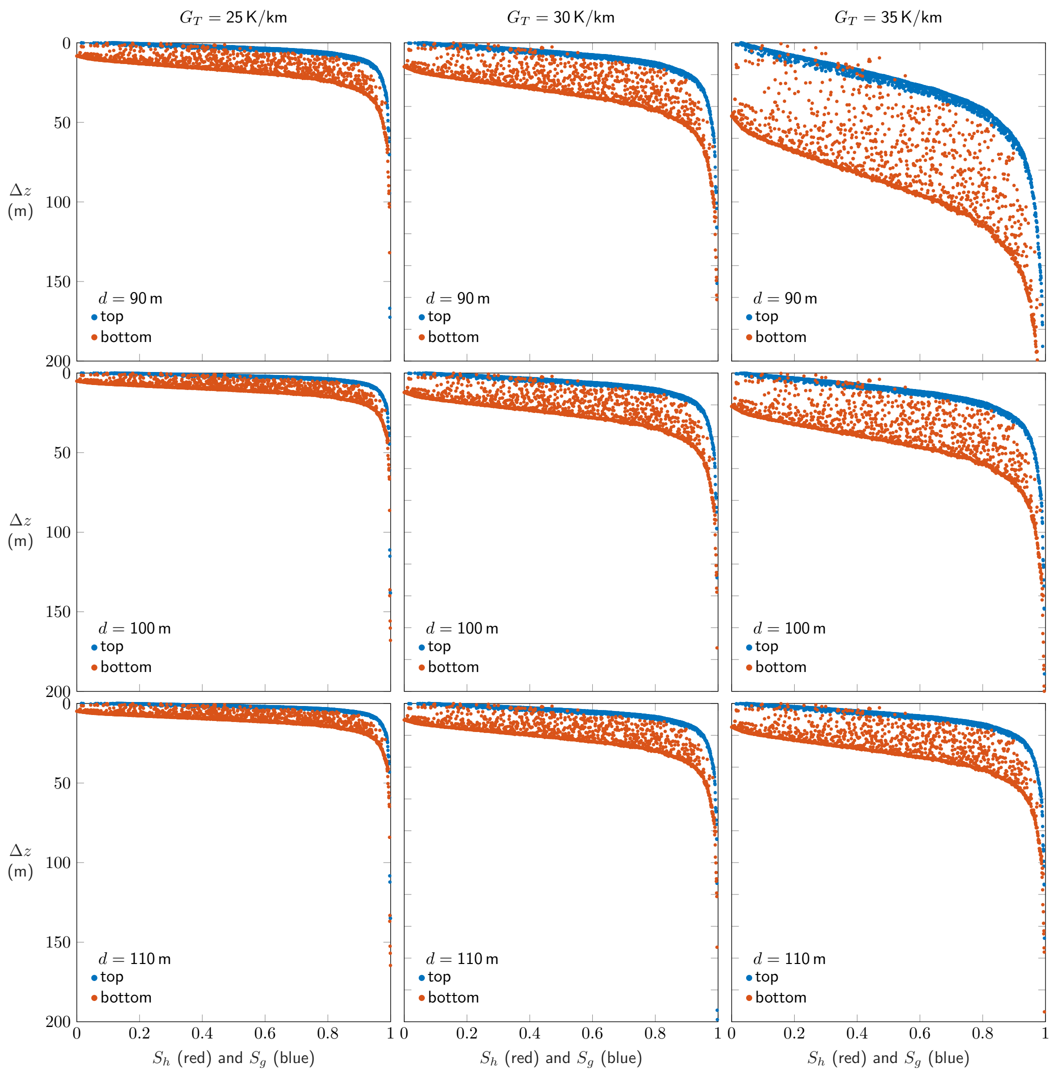

Figure 3. Sensitivity of the three-phase zone to the variations of water depth d and geothermal gradient G_T for a grain radius 10^{-5} m. The three-phase zone becomes broader and deeper with shallower d and larger G_T, which means the zone is not well constrained. With a water depth $d = 90$ m and a geothermal gradient $G_T = 35$ K/km (upper right tile), the three-phase zone entirely encompasses the L_{CO_2}-G boundary.

4.3 Rate of hydrate formation in the three-phase zone

In advection-dominated hydrate formation, methane hydrate reservoir evolves at a timescale of hundreds of thousands years because of the slow migration of methane. For CO_2 sequestration site, however, the three-phase zone is close to the L_{CO_2}-G boundary, and the relevant Péclet number is smaller than unity, so hydrate formation in the three-phase zone is mainly determined by CO_2 diffusion. In the case of broad three-phase zones, the three-phase zone may directly encompass the L_{CO_2}-G boundary. After the initial nucleation stage, the characteristic size of hydrate crystal is $\sqrt{D_g t}$ (Zener, 1949), so with $D_g \sim 10^{-9}\,\mathrm{m}^2/\mathrm{s}$, the crystal can grow to a size comparable to the pore size in the sediments in a very short period of time with abundant CO_2 supply, leading to fast-forming sealing capability by CO_2 hydrates.

4.4 Hydrate in equilibrium with the liquid CO_2

In previous sections we only considered the situations where the CO_2 hydrate is in equilibrium with gaseous or aqueous CO_2, and neglected the situation where the CO_2 hydrate is in equilibrium with the liquid CO_2. In actual practice of sub-seabed CO_2 sequestration, CO_2 hydrate may form during the liquid CO_2 injection (Kvamme et al., 2019). However, for the temperature and pressure range for our consideration, the only instance where hydrate may form in equilibrium with liquid CO_2 in the absense of promoters or inhibitors is at the L_{CO_2}-G boundary (Figure 1a), with a specific depth at z_v. At this depth liquid CO_2 can turn into gaseous CO_2 or CO_2 hydrate, and the hydrate can further reduce the permeability and strengthen the sealing capability. Some recent experimental studies (e.g., Qureshi et al., 2022) suggested that high pressure liquid CO_2 can form hydrate much faster due to higher driving force, but more understanding of the multiphase flow of liquid CO_2 and seawater in sub-seabed environment is needed before better assessment can be made.

4.5 Effects of hydrate promoters

Many proposed CO_2 sequestration technologies involve hydrate promoters, including thermodynamic promoters and kinetic promoters. Thermodynamic promoters may shift the phase equilibrium of hydrate, but are not environmentally friendly, whereas kinetic promoters, especially those which are environmentally friendly, generally do not alter the hydrate equilibrium (Nashed et al., 2018). As a result, we expect that the kinetic hydrate promoters will not change the depth of the BHSZ, as well as the three-phase coexisting zone.

5 Conclusion

Self-sealing capability of the CO_2 hydrate-bearing sediment layer is crucial to effective sequestration of CO_2 in sub-seabed sediment, and the three-phase zone plays a critical role in the formation of the self-sealing cap. We demonstrate that unlike methane hydrate reservoir which takes a long time to form, the self-sealing cap above the CO_2 sequestration site can form in a relatively short period due to enhanced CO_2 permeation and permeability reduction in the three-phase zone by CO_2 bubbles and hydrate crystals. With typical geological settings, we use a Monte Carlo method to simulate the depth and thickness of the three-phase zone, which exists below the bulk BHSZ and is close to the CO_2 liquid—gas boundary less than 100 m away from the BHSZ. The three-phase zone becomes broader and deeper with finer grains, shallower water depths and larger geothermal gradients, suggesting possible variations in the sealing capability when submarine earthquakes or landslides occur. Our work provides an insight into the development of sealing capability of the CO_2 hydrate-bearing sediment cap, distinguishes its difference from the methane hydrate reservoir, and sheds light on other mechanisms related to CO_2 hydrate accumulation above sequestration sites.

Acknowledgments

J.C. and S.M. were supported by Chinese Academy of Sciences (No. QYZDY-SSW-DQC029), and J.C. was also supported by the National Natural Science Foundation of China (Grant No. 41804085).

Open Research

The relevant python scripts and data can be found on https://doi.org/10.5281/zenodo.6559009, open sourced under the MIT license.

References

Adams, E. E., & Caldeira, K. (2008, October). Ocean storage of co2. *Elements*, *4*(5), 319–324. doi: 10.2113/gselements.4.5.319

Anderson, G. K. (2003, July). Enthalpy of dissociation and hydration number of carbon dioxide hydrate from the clapeyron equation. *J. Chem. Thermodyn.*, *35*(7), 1171–1183. doi: 10.1016/s0021-9614(03)00093-4

Burwicz, E., Reichel, T., Wallmann, K., Rottke, W., Haeckel, M., & Hensen, C. (2017, May). 3-d basin-scale reconstruction of natural gas hydrate system of the green canyon, gulf of mexico. *Geochem. Geophys. Geosyst.*, *18*(5), 1959–1985. doi: 10.1002/2017gc006876

Carroll, J. J., Slupsky, J. D., & Mather, A. E. (1991, November). The solubility of carbon dioxide in water at low pressure. *J. Phys. Chem. Ref. Data*, *20*(6), 1201–1209. doi: 10.1063/1.555900

Chen, J., Mei, S., Irizarry, J. T., & Rempel, A. W. (2020, October). A monte carlo approach to approximating the effects of pore geometry on the phase behavior of soil freezing. *J. Adv. Model. Earth Syst.*, *12*(10). doi: 10.1029/2020ms002117

Chen, J., Rempel, A. W., & Mei, S. (2021, February). A monte carlo model of gas-liquid-hydrate three-phase coexistence constrained by pore geometry in marine sediments. *Front. Earth Sci.*, *8*(718). doi: 10.3389/feart.2020.600733

Clennell, M. B., Hovland, M., Booth, J. S., Henry, P., & Winters, W. J. (1999, October). Formation of natural gas hydrates in marine sediments: 1. conceptual model of gas hydrate growth conditioned by host sediment properties. *J. Geophys. Res. Solid Earth*, *104*(B10), 22985–23003. doi: 10.1029/1999jb900175

Daigle, H., & Dugan, B. (2011, January). Capillary controls on methane hydrate distribution and fracturing in advective systems. *Geochem. Geophys. Geosyst.*, *12*(1). doi: 10.1029/2010gc003392

Davie, M. K., & Buffett, B. A. (2003, January). Sources of methane for marine gas hydrate: inferences from a comparison of observations and numerical models. *Earth Planet. Sci. Lett.*, *206*(1-2), 51–63. doi: 10.1016/s0012-821x(02)01064-6

Dickens, G. R., & Quinby-Hunt, M. S. (1994, September). Methane hydrate stability in seawater. *Geophys. Res. Lett.*, *21*(19), 2115–2118. doi: 10.1029/94gl01858

Duan, Z., & Sun, R. (2003, February). An improved model calculating co2 solubility in pure water and aqueous NaCl solutions from 273 to 533 k and from 0 to 2000 bar. *Chem. Geol.*, *193*(3-4), 257–271. doi: 10.1016/s0009-2541(02)00263-2

Eccles, J. K., & Pratson, L. (2012, October). Global co2 storage potential of self-sealing marine sedimentary strata. *Geophys. Res. Lett.*, *39*(19). doi: 10.1029/2012gl053758

Espinoza, D. N., & Santamarina, J. C. (2010, July). Water-co2-mineral systems: Interfacial tension, contact angle, and diffusion-implications to co2 geological storage. *Water Resour. Res.*, *46*(7). doi: 10.1029/2009wr008634

Fenghour, A., Wakeham, W. A., & Vesovic, V. (1998, January). The viscosity of carbon dioxide. *J. Phys. Chem. Ref. Data*, *27*(1), 31–44. doi: 10.1063/1.556013

Finney, J. L. (1970, November). Random packings and the structure of simple liquids. i. the geometry of random close packing. *Proc. R. Soc. London, Ser. A*, *319*(1539), 479–493. doi: 10.1098/rspa.1970.0189

Goldberg, D. S., Takahashi, T., & Slagle, A. L. (2008, July). Carbon dioxide sequestration in deep-sea basalt. *Proc. Natl. Acad. Sci.*, *105*(29), 9920–9925. doi: 10.1073/pnas.0804397105

Hardy, S. C. (1977, February). A grain boundary groove measurement of the surface tension between ice and water. *Philos. Mag.*, *35*(2), 471–484. doi: 10.1080/14786437708237066

Henry, P., Thomas, M., & Clennell, M. B. (1999, October). Formation of natural gas hydrates in marine sediments: 2. thermodynamic calculations of stability conditions in porous sediments. *J. Geophys. Res. Solid Earth*, *104*(B10), 23005–23022. doi: 10.1029/1999jb900167

Koide, H., Shindo, Y., Tazaki, Y., Iijima, M., Ito, K., Kimura, N., & Omata, K. (1997, January). Deep sub-seabed disposal of co2 – the most protective storage –. *Energy Convers. Manage.*, *38*, S253–S258. doi: 10.1016/s0196-8904(96)00278-6

Kvamme, B., Aromada, S. A., & Saeidi, N. (2019, September). Heterogeneous and homogeneous hydrate nucleation in co2/water systems. *J. Cryst. Growth*, *522*, 160–174. doi: 10.1016/j.jcrysgro.2019.06.015

Larson, S. D. (1955). *Phase studies of the two component carbon dioxide-water system involving the carbon dioxide hydrate* (Doctoral dissertation). University of Illinois, Urbana, IL.

Levine, J. S., Matter, J. M., Goldberg, D., Cook, A., & Lackner, K. S. (2007, December). Gravitational trapping of carbon dioxide in deep sea sediments: Permeability, buoyancy, and geomechanical analysis. *Geophys. Res. Lett.*, *34*(24). doi: 10.1029/2007gl031560

Li, Z., Dong, M., Li, S., & Huang, S. (2006, July). CO2 sequestration in depleted oil and gas reservoirs—caprock characterization and storage capacity. *Energ. Convers. Manage.*, *47*(11-12), 1372–1382. doi: 10.1016/j.enconman.2005.08.023

Liu, X., & Flemings, P. B. (2011, July). Capillary effects on hydrate stability in marine sediments. *J. Geophys. Res. Solid Earth*, *116*(B7). doi: 10.1029/2010jb008143

Masson-Delmotte, V., Zhai, P., Pirani, A., Connors, S. L., Péan, C., Berger, S., … Zhou, B. (2021). *Ipcc, 2021: Climate change 2021: The physical science basis. contribution of working group i to the sixth assessment report of the intergovernmental panel on climate change.*

Metz, B., Davidson, O., De Coninck, H. C., Loos, M., & Meyer, L. (2005). *Ipcc special report on carbon dioxide capture and storage.* Cambridge University Press.

Nashed, O., Partoon, B., Lal, B., Sabil, K. M., & Shariff, A. M. (2018, July). Review the impact of nanoparticles on the thermodynamics and kinetics of gas hydrate formation. *J. Nat. Gas Sci. Eng.*, *55*, 452–465. doi: 10.1016/j.jngse.2018.05.022

Nevers, N. (2012). *Physical and chemical equilibrium for chemical engineers.* Hoboken, N.J: Wiley.

Nole, M., Daigle, H., Cook, A. E., Malinverno, A., & Flemings, P. B. (2018, October). Burial-driven methane recycling in marine gas hydrate systems. *Earth Planet. Sci. Lett.*, *499*, 197–204. doi: 10.1016/j.epsl.2018.07.036

Peng, D.-Y., & Robinson, D. B. (1976, February). A new two-constant equation of state. *Ind. Eng. Chem. Fundam.*, *15*(1), 59–64. doi: 10.1021/i160057a011

Qureshi, M. F., Dhamu, V., Usadi, A., Barckholtz, T. A., Mhadeshwar, A. B., & Linga, P. (2022, January). CO2 hydrate formation kinetics and morphology observations using high-pressure liquid CO2 applicable to sequestration. *Energ. Fuel.*. doi: 10.1021/acs.energyfuels.1c03840

Reagan, M. T., & Moridis, G. J. (2008, December). Dynamic response of oceanic hydrate deposits to ocean temperature change. *J. Geophys. Res.*, *113*(C12). doi: 10.1029/2008jc004938

Rempel, A. W. (2012, April). Hydromechanical processes in freezing soils. *Vadose Zone J.*, *11*(4), 0. doi: 10.2136/vzj2012.0045

Rempel, A. W., & Buffett, B. A. (1997, May). Formation and accumulation of gas hydrate in porous media. *J. Geophys. Res. Solid Earth*, *102*(B5), 10151–10164. doi: 10.1029/97jb00392

Rutqvist, J., & Moridis, G. J. (2009, May). Numerical studies on the geomechanical stability of hydrate-bearing sediments. *SPE J.*, *14*(02), 267–282. doi: 10.2118/126129-pa

Schmidt, C., Gupta, S., Rüpke, L., Burwicz-Galerne, E., & Hartz, E. H. (2022, June). Sedimentation-driven cyclic rebuilding of gas hydrates. *Mar. Petrol. Geol.*, *140*, 105628. doi: 10.1016/j.marpetgeo.2022.105628

Shukla, R., Ranjith, P., Haque, A., & Choi, X. (2010, October). A review of studies on CO2 sequestration and caprock integrity. *Fuel*, *89*(10), 2651–2664. doi: 10.1016/j.fuel.2010.05.012

Sloan, E. D., & Koh, C. (2007). *Clathrate hydrates of natural gases.* CRC press.

Spivey, J. P., McCain, W. D., & North, R. (2004, July). Estimating density, formation volume factor, compressibility, methane solubility, and viscosity for oilfield brines at temperatures from 0 to 275 °c, pressures to 200 MPa, and salinities to 5.7 mole/kg. *J. Can. Pet. Technol.*, *43*(07). doi: 10.2118/04-07-05

Sultan, N., Cochonat, P., Foucher, J.-P., & Mienert, J. (2004, December). Effect of gas hydrates melting on seafloor slope instability. *Mar. Geol.*, *213*(1-4), 379–401. doi: 10.1016/j.margeo.2004.10.015

Sun, R., & Duan, Z. (2005, September). Prediction of ch4 and co2 hydrate phase equilibrium and cage occupancy from ab initio intermolecular potentials. *Geochim. Cosmochim. Acta*, *69*(18), 4411–4424. doi: 10.1016/j.gca.2005.05.012

Tohidi, B., Anderson, R., Clennell, M. B., Burgass, R. W., & Biderkab, A. B. (2001, September). Visual observation of gas-hydrate formation and dissociation in synthetic porous media by means of glass micromodels. *Geology*, *29*(9), 867. doi: 10.1130/0091-7613(2001)029⟨0867:vooghf⟩2.0.co;2

Udachin, K. A., Ratcliffe, C. I., & Ripmeester, J. A. (2001, May). Structure, composition, and thermal expansion of co2hydrate from single crystal x-ray diffraction measurements. *J. Phys. Chem. B*, *105*(19), 4200–4204. doi: 10.1021/jp004389o

Wagner, W., & Pruss, A. (1993, May). International equations for the saturation properties of ordinary water substance. revised according to the international temperature scale of 1990. addendum to j. phys. chem. ref. data 16, 893 (1987). *J. Phys. Chem. Ref. Data*, *22*(3), 783–787. doi: 10.1063/1.555926

Waite, W. F., Santamarina, J. C., Cortes, D. D., Dugan, B., Espinoza, D. N., Germaine, J., … others (2009, December). Physical properties of hydrate-bearing sediments. *Rev. Geophys.*, *47*(4). doi: 10.1029/2008rg000279

Wendland, M., Hasse, H., & Maurer, G. (1999, September). Experimental pressure-temperature data on three- and four-phase equilibria of fluid, hydrate, and ice phases in the system carbon dioxide-water. *J. Chem. Eng. Data*, *44*(5), 901–906. doi: 10.1021/je980208o

Wilder, J. W., Seshadri, K., & Smith, D. H. (2001, October). Modeling hydrate formation in media with broad pore size distributions. *Langmuir*, *17*(21), 6729–6735. doi: 10.1021/la010377y

You, K., & Flemings, P. B. (2021, April). Methane hydrate formation and evolution during sedimentation. *J. Geophys. Res. Solid Earth*, *126*(4). doi: 10.1029/2020jb021235

You, K., Flemings, P. B., Malinverno, A., Collett, T. S., & Darnell, K. (2019, October). Mechanisms of methane hydrate formation in geological systems. *Rev. Geophys.*. doi: 10.1029/2018rg000638

Zener, C. (1949, October). Theory of growth of spherical precipitates from solid solution. *J. Appl. Phys.*, *20*(10), 950–953. doi: 10.1063/1.1698258

Figure1a.

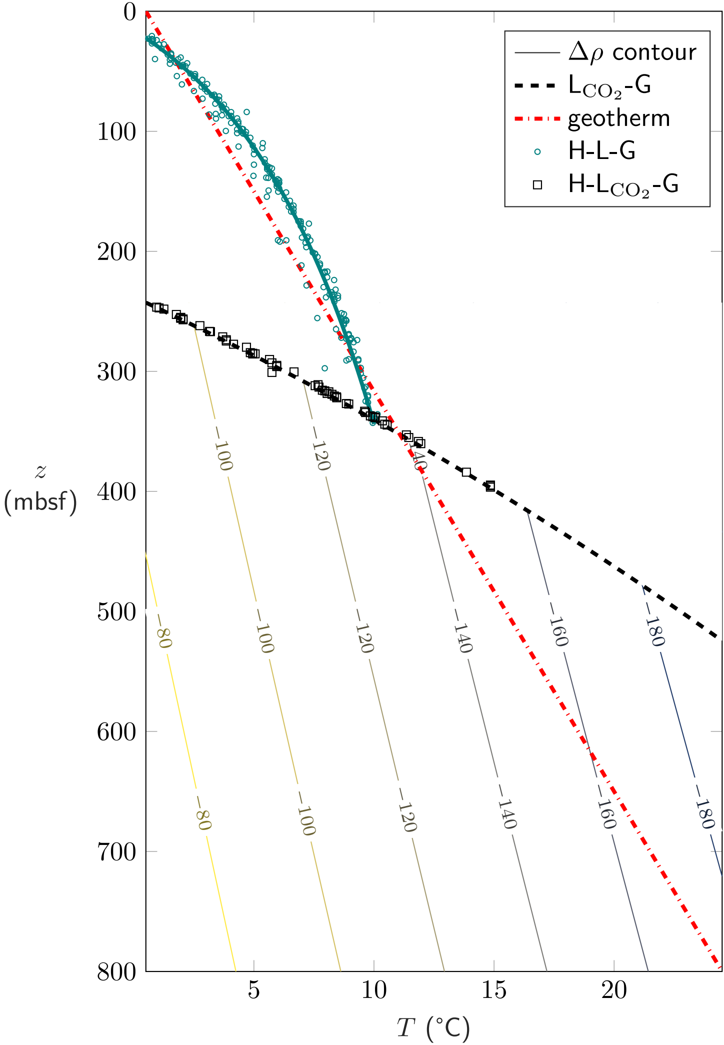

Δρ contour
L$_{CO_2}$-G
geotherm
H-L-G
H-L$_{CO_2}$-G
z (mbsf)
T (°C)
0
100
200
300
400
500
600
700
800
5
10
15
20
−80
−100
−120
−140
−160
−180

Figure1b.

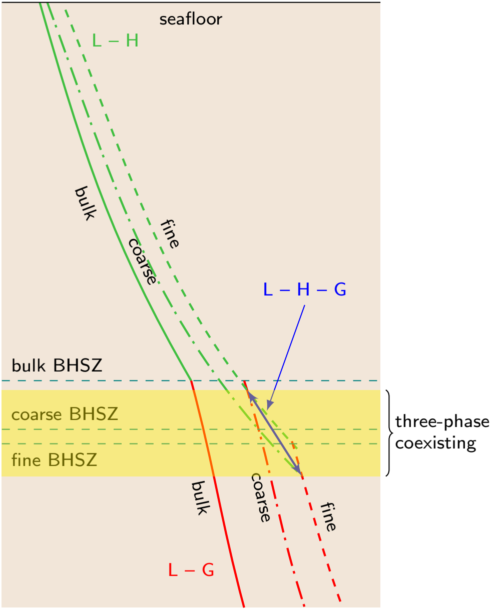
seafloor
L – H
bulk
coarse
fine
L – H – G
bulk BHSZ
coarse BHSZ
fine BHSZ
three-phase
coexisting
bulk
coarse
fine
L – G

Figure2.

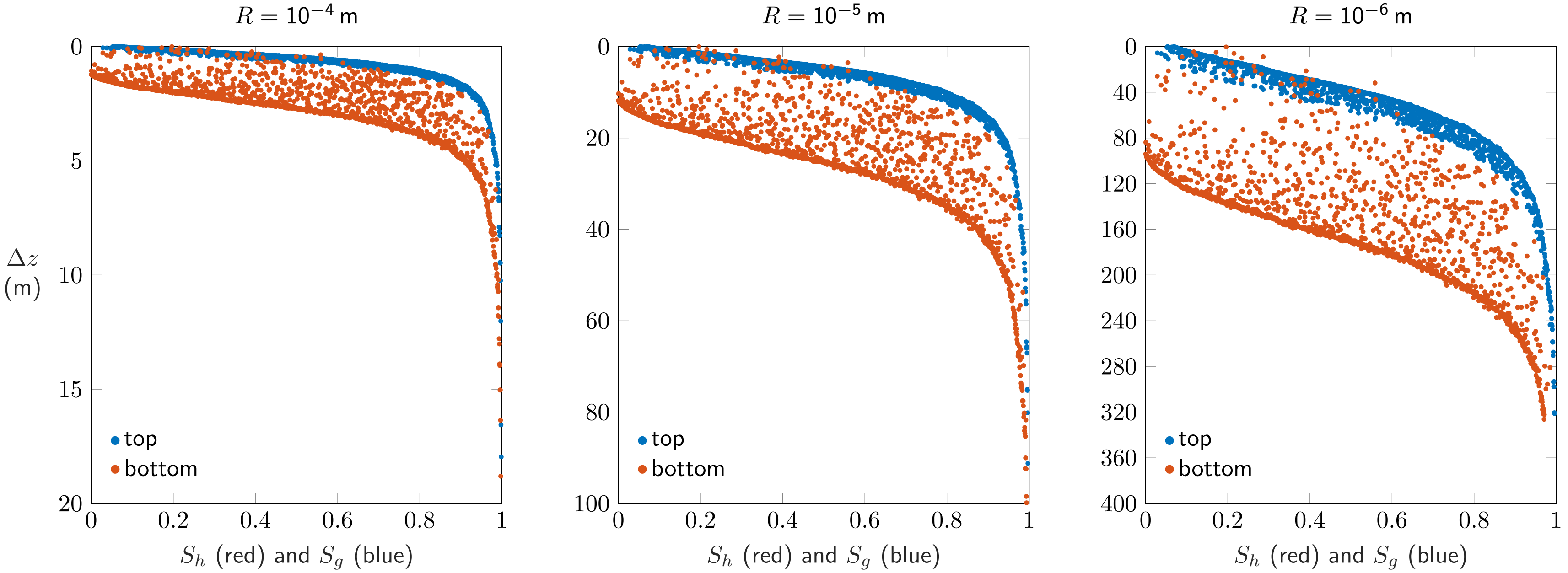

$R = 10^{-4}$ m
$R = 10^{-5}$ m
$R = 10^{-6}$ m
Δz (m)
top
bottom
S_h (red) and S_g (blue)
0
5
10
15
20
0.2
0.4
0.6
0.8
1
40
60
80
100
120
160
200
240
280
320
360
400

Figure3.

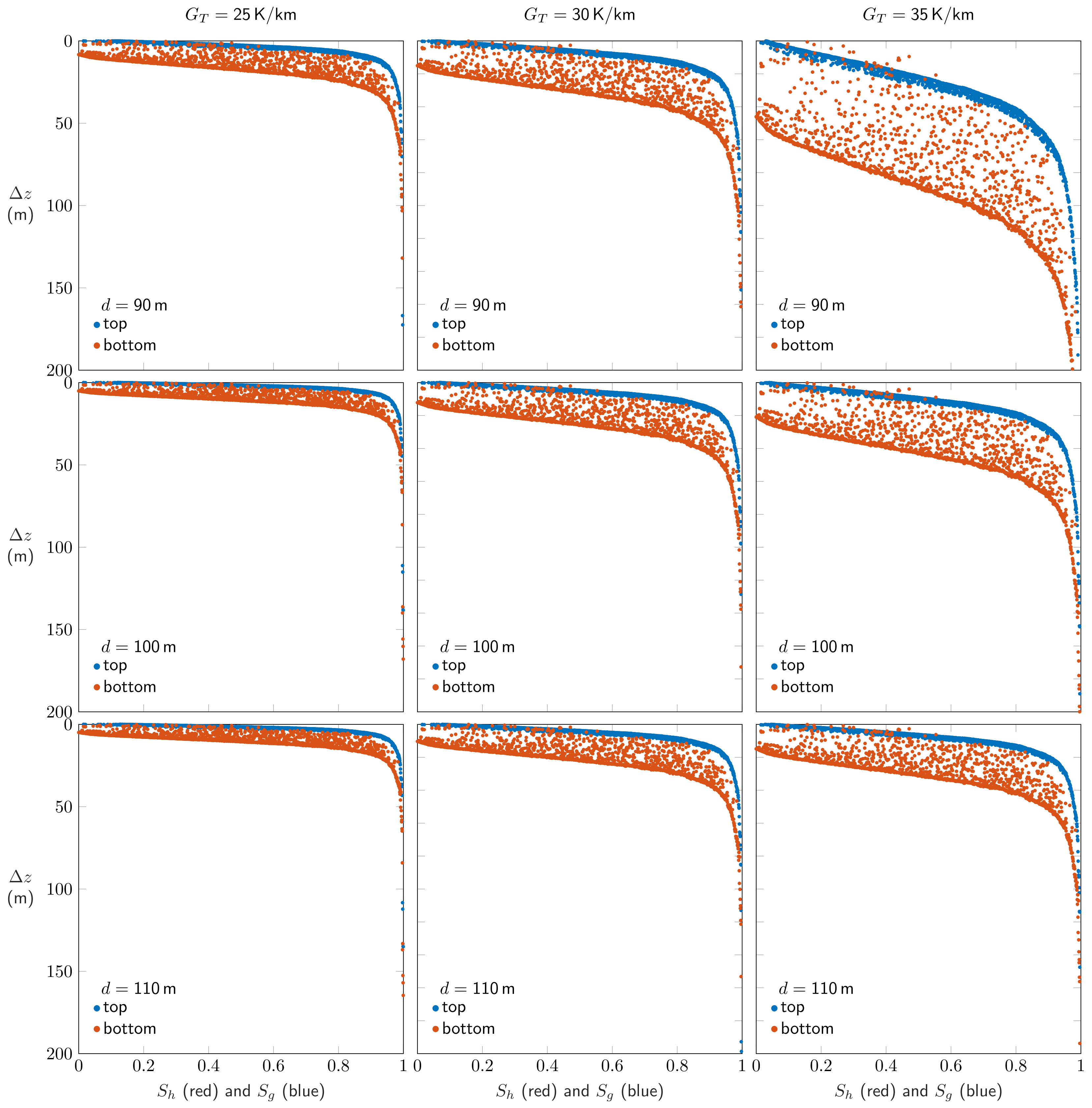

$G_T = 25$ K/km
$G_T = 30$ K/km
$G_T = 35$ K/km
Δz (m)
$d = 90$ m
$d = 100$ m
$d = 110$ m
top
bottom
0
50
100
150
200
0
0.2
0.4
0.6
0.8
1
S_h (red) and S_g (blue)

FigureS1b.

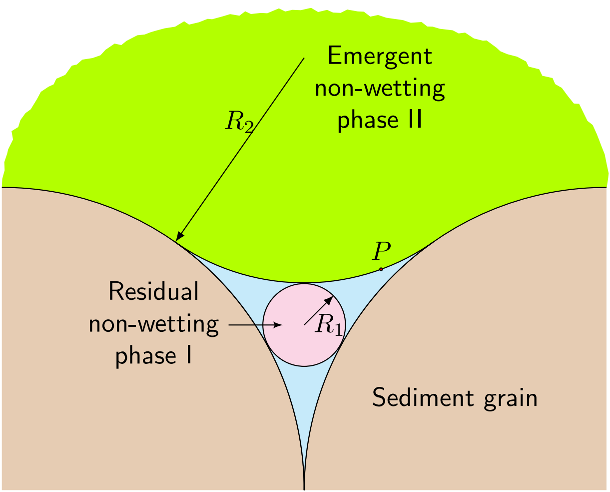
Emergent
non-wetting
phase II
R_2
P
Residual
non-wetting
phase I
R_1
Sediment grain

FigureS1a.

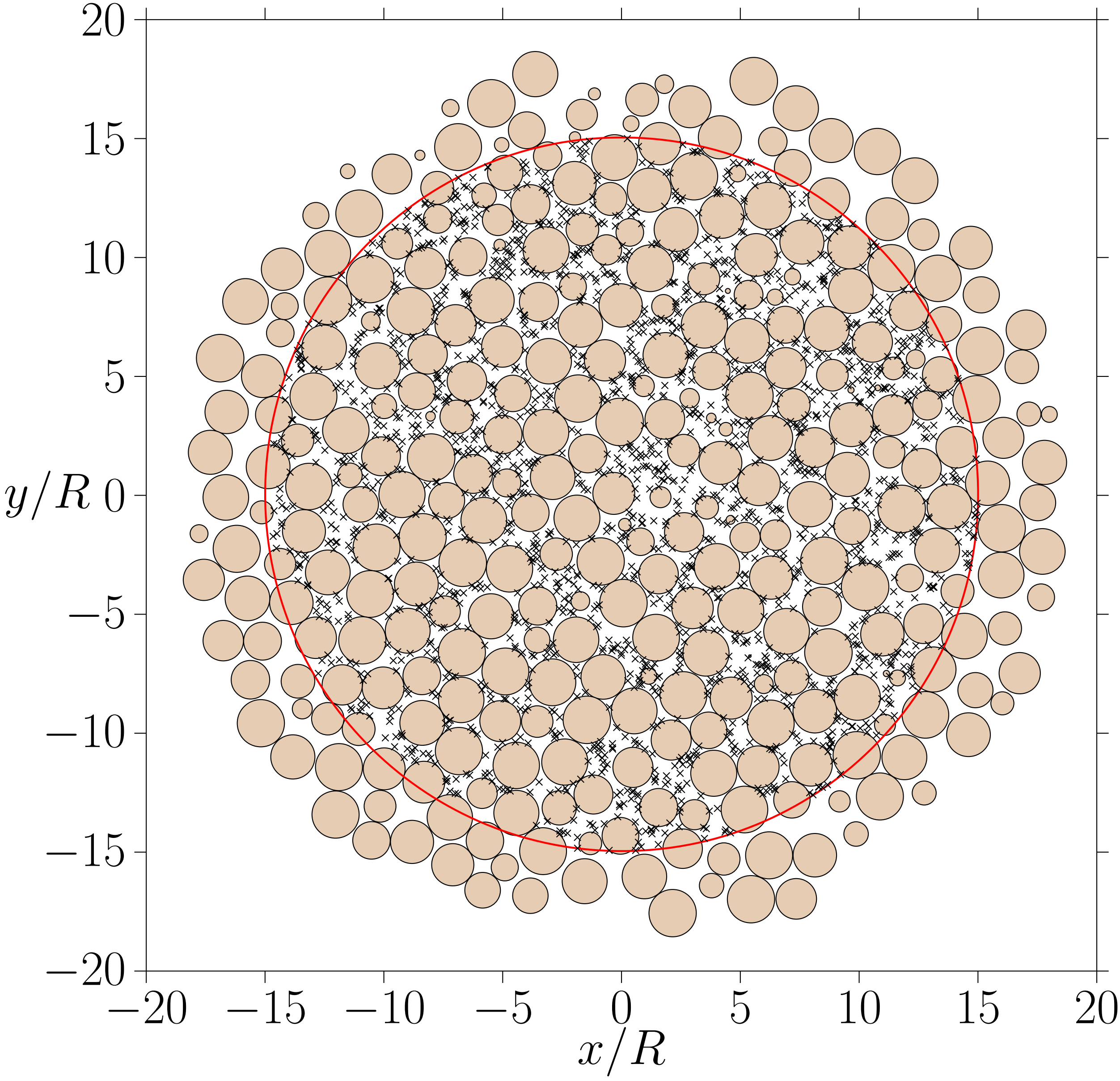
20
15
10
5
0
−5
−10
−15
−20
y/R
−20
−15
−10
−5
0
5
10
15
20
x/R